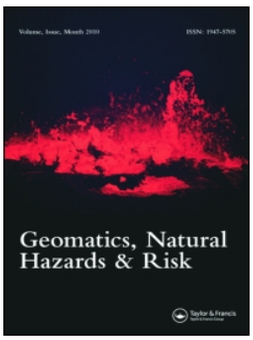

Geomatics, Natural Hazards and Risk

ISSN: 1947-5705 (Print) 1947-5713 (Online) Journal homepage: https://www.tandfonline.com/loi/tgnh20

Measuring the volume of flushed sediments in a reservoir using multi-temporal images acquired with UAS

D. Pagliari, L. Rossi, D. Passoni, L. Pinto, C. De Michele & F. Avanzi

To cite this article: D. Pagliari, L. Rossi, D. Passoni, L. Pinto, C. De Michele & F. Avanzi (2017) Measuring the volume of flushed sediments in a reservoir using multi-temporal images acquired with UAS, Geomatics, Natural Hazards and Risk, 8:1, 150-166, DOI: 10.1080/19475705.2016.1188423

To link to this article: https://doi.org/10.1080/19475705.2016.1188423

Published online: 27 May 2016.

GEOMATICS, NATURAL HAZARDS AND RISK, 2017
VOL. 8, NO. 1, 150–166
http://dx.doi.org/10.1080/19475705.2016.1188423

Taylor & Francis
Taylor & Francis Group

Measuring the volume of flushed sediments in a reservoir using multi-temporal images acquired with UAS

D. Pagliari[a], L. Rossi[a], D. Passoni[b], L. Pinto[a], C. De Michele[a] and F. Avanzi[a]

[a]Department of Civil and Environmental Engineering, Politecnico di Milano, Milano, Italy; [b]Department of Civil, Chemistry and Environmental Engineering, Università degli Studi di Genova, Genova, Italy

ABSTRACT

We compute the volume of flushed sediments in a dam using photogrammetry-based multi-temporal surveys with an unmanned aerial system (UAS). Coping with sediments accumulation and erosion in reservoir is a living topic in modern hydraulics of dams, since the increase of sediment may reduce the reservoir capacity, endanger dam's stability, and represent an economical loss. As a result, a number of remedies can be considered, such as flushing or mechanical removal. To evaluate the performance of these operations, measuring the volume of removed sediments and their spatial distribution is important. Here, we show that photogrammetry from UASs represents a suitable solution to reckon the volume of removed sediments. The case study is the Fusino dam (Lombardia region, Northern Italy). Two surveys were performed, before and after sediment removal. In both cases, the flight has been planned with an average flight height equal to 65 m, leading to a mean ground sample distance (GSD) equal to 0.013 m. The 22 ground control points (GCP) used to adjust the photogrammetric block were measured with both global navigation satellite system (GNSS) and a total station. Each survey produced a cloud of about 40 million of points. Moreover, the digital surface model (DSM) produced by each photogrammetric flight has been validated with sample points measured with a robotic total station. Results show high consistency between computed DSMs and validation dataset, with a mean height difference equal, respectively, to 0.003 and −0.004 m considering the two different surveys, with a standard deviation around 0.05 m in both the cases. The volume of sediments flushed was estimated to be about 26,000 m^3, which represents about 2%–3% of the total reservoir capacity. We estimated also a 6% difference in terms of reservoir capacity between the present condition and the no-sediments condition.

ARTICLE HISTORY
Received 9 November 2015
Accepted 1 May 2016

KEYWORDS
Photogrammetry; dam; UAS; flushing; validation

1. Introduction

Dams and reservoirs represent engineering works that segment the rivers and regulate water (Graf 1999). They modify the water dynamics permitting its use for several purposes like civil use, irrigation, food and energy production, or industrial activities. The importance of reservoirs is expected to increase in the next years with the increasing of population, economic activity, and water demand. These engineering works alter also the sediment dynamics transported by water. Sediments play a fundamental role in the hydrological, geomorphological and ecological dynamics of rivers (Owens et al. 2005). They also maintain fluvial environment like floodplains, wetlands, and estuaries, and

CONTACT D. Pagliari diana.pagliari@polimi.it

guarantee equilibrium between processes of erosion and deposition that usually occur along the rivers (Morris & Fan 1998).

The dam operates a shift in sediment dynamics of the river, accumulating the solid material behind the dam, and preventing the sediments to supply fluvial areas downstream, thus acting as sediment buffers (Kummu & Varis 2007). This causes an excess of sediment deposit upstream and a lack of sediments downstream, which the river attempts to restore modifying its geometry (Annandale 1987; Yang et al. 2011; Lewis et al. 2013).

Some sediment-related problems occur, both upstream and downstream the dams (Poff & Hart 2002). These problems include the reduction of the lifetime of the reservoir, obstruction of intakes, damages to machineries (e.g. turbines), and loss of hydropower production. Sedimentation is considered the principal cause of life reduction for many dams around the world. Mahmood (1987) estimated that 50 km^3/yr is the sediment rate trapped by all the dams worldwide, representing around 1% of global reservoir storage capacity. Palmieri et al. (2003) found a similar result with a rate of 45 km^3/yr, i.e. representing around 0.8% of global reservoir storage capacity. However, sedimentation rates are geographically different. In China, there are 82,000 reservoirs, which have an average annual rate of lost storage capacity of 2.3%, i.e. the highest rate of loss in the world Zhou (1993). In the US, large reservoirs have an average rate of around 0.2%, with variations between 0.5% in Pacific states and 0.1% in the Northeast states. Exemplary is the case of Camar reservoir in Venezuela reported by Morris and Fan (1998), where the structure lost completely its storage capacity, in less than 15 years. In Italy, Surian et al. (2009) reported that the dams along the Piave river (North-Eastern Italy) have reduced the sediment load from 1.00×10^6 to 1.45×10^5 m^3/yr.

Palmieri et al. (2003) have estimated the cost of sedimentation at world scale in 13 billion USD/yr, needed to replace the lost storage. According to Basson (2010), most of the existing reservoirs in the world could be completely silted up in 200−300 years from now. The progressive sedimentation behind the dam constitutes a risk of functioning failure, thus the sediment volume must be monitored in order to make a proper management of the structure. These issues are paramount in conditions of climate change. In fact, modifications in the stability of frozen (or thawed) soils and/or glaciers may result in an increase of sediment production (Hallet et al. 1996; Leeder et al. 1998). Clearly, a reduction of reservoir volume may also represent an economical loss, due to a reduction in the regulation capability of dams.

To cope with sedimentation and to partially restore reservoir capacity, different types of techniques have been considered in the past. An example is flushing (Fruchard & Camenen 2012; Kondolf et al. 2014), i.e. an hydraulic removal of sediments. Other examples are sediment trapping or bypass, sluicing or mechanical excavation (see Kondolf et al. (2014) for an exhaustive review on this topic).

In order to evaluate the performance of these techniques, the volume of flushed (or removed) sediment has to be measured. Sediment volume is generally measured using bathymetric soundings (Kummu & Varis 2007; Furnans & Austin 2008; Yang et al. 2011), acoustic profiling (Dunbar et al. 1999), sediment cores (Van Metre et al. 1997), etc. Another source of information are measurements of sediment discharges (Yang et al. 2011), or measurements of incoming and outcoming suspended solids at a dam during relevant rainfall and runoff events (Lewis et al. 2013), or at pre-dam and post-dam river sites (Kummu & Varis 2007). An alternative is the use of empirical equations estimating the amount of inflowing sediment that is trapped permanently in a reservoir, the so-called trapping efficiencies estimators (Lewis et al. 2013). Some examples are those by Churchill (1948) and Brune (1953). However, Trimble and Bube (1990) argue that sediment yield data are often unreliable, unless they are not sampled continuously over a long period, while reservoirs trap efficiency may be actually a relevant unknown. An example of work dealing with the measurement of flushing erosion is Jansson and Erlingsson (2000). The paper focuses on a case study of flushing in Costa Rica. In that case, the volume of eroded sediment was measured using depth surveys.

An ideal condition to measure the volume of sediments in a reservoir occurs when it is empty. Such a condition occurs periodically during the lifetime of a reservoir due to maintenance reasons (e.g. during sediment removal operations) and seasonality of streamflow and energy demand. In

these situations, several survey techniques may allow a 3D reconstruction of the digital surface model (DSM) of the existing surface of the reservoir (sediments included). By repeating this procedure periodically, the volume of flushed sediment can be monitored by means of DSMs differentiation. This represents a simple way to evaluate the performance and expected impacts of this remediation strategy.

Here, we test the use of photogrammetry-based surveys by means of unmanned aerial system (UAS) to recover the volume of flushed sediments in a dam. UASs are fast and automatic in performing the surveys. Therefore, they may represent a competitive solution to obtain a precise reconstruction of sediment dynamics.

The use of UAS photogrammetry surveys allows having a more flexible acquisition phase, with respect to that realized from airplanes and helicopters. On the other hand, the final precisions are lower than the ones that could be reached acquiring images at the same scale using aircrafts, even if they are very high in absolute terms. This is mainly due to the low quality of the optics of the mass-market cameras usually installed onboard UASs. Thanks to the use of gimbals, it is possible to vary the inclination of the optic sensor, allowing to control in a better way the acquisition geometry and having configurations similar to those of close-range photogrammetry. Nocerino et al. (2013) show how it is possible to improve the final accuracy by adding oblique images to the nadir ones. The most noticeable effect is in the height component. In recent years, Structure from Motion (SfM) techniques have become a standard for close-range photogrammetry, allowing the combination of the rigorous mathematical models of classical photogrammetry with the high level of automation and matching techniques typically of computer vision (Roncella et al. 2011). SfM has introduced in modern photogrammetry a number of algorithms capable of extracting and matching a high number of tie points, even in case of images acquired with large-scale variations or from different viewpoints, expanding its use to a larger amount of users. SfM differs from traditional photogrammetry because the camera alignment and the scene geometry are solved simultaneously in a highly redundant bundle block adjustment, using a high number of automatic extracted observations and without the need of a priori information (Westoby et al. 2012). It requires an image dataset with a high level of overlapping and the solution is usually computed in free-network adjustment; the alignment to the object space coordinate system is usually performed in a second separate step, requiring a lower number of GCPs. A review of the differences between SfM and classical photogrammetry, focused on DSMs creation, is discussed in Fonstad et al. (2013). In UAS acquisitions, it is frequent to have strong variation in the number of overlapping images, because of the poor stability of the platform itself. This can result in a failure of the SfM used to orientate the photogrammetric block. This problem is usually overcome by increasing the longitudinal and transversal overlapping. Usually, the along-track overlapping is about 70%−90%, while the one along the cross-track direction is about 60%−90% (Skarlatos et al. 2015).

2. State of the art of surveying techniques

Three-dimensional survey of a dam requires precision, accuracy, repeatability, low-cost, and easy of usedness. Different survey methods have been developed in order to fulfil these requirements. In González-Aguilera et al. (2008), three methods are considered: classical topographic methods, global navigation satellite systems (GNSS) and digital photogrammetry. Terrestrial laser scanner (TLS) may be another possible solution, since it allows creating dense point clouds also at great distances (Alba et al. 2006). The DSM has to be determined with a high level of detail, if the objective is the morphology of a reservoir closed by a dam. The DSM can be determined in a multi-temporal way by comparing different surveys at different epochs and using these data to estimate surface variations, as well as volume of eroded or deposited material. In order to repeat the survey, it is necessary to locally monument the reference system using station points that must be located in stable areas in case of classical topographic or GNSS methods or by placing targets that can be easily identified in the acquired images in case of photogrammetry or in the point clouds in case of TLS. The

material and the dimensions of the targets have to be carefully chosen considering the type of survey. For TLS, the material and the shape of the targets have to guarantee an optimal response to the laser light source. At the same time, they have to be easily identifiable in the surveyed scene (Alba et al. 2006). As for the photogrammetric targets, they have to be characterized by shape, colour and dimensions that allow identifying them univocally, preferable with an automatic procedure (Clarke 1994). These ground control points (GCPs) have to be surveyed with an accuracy that is strictly related with the expected precision of the reservoir model. Often a simple real-time kinematic (RTK) GNSS survey may not be sufficient to reach the requested accuracy. Instead, it will be necessary to measure those GCPs, including them in a network where static GNSS measurements (if the points are not visible from one to another) and/or total station measurements are used.

The reconstruction of the morphology of a reservoir requires a huge number of points, thus some of the methods already discussed are not feasible because it would be necessary to station on all the surveyed points, e.g. using total station or GNSS. This problem could be overcome only using a robotic total station featured with an electronic distance meter (EDM) that does not require a retroreflective prism and, practically, acquires a high precision dense point cloud.

The classical topographic method consists in the measurement of angles and distances, using a total station. Recently, Leica released on the market the MultiStation (Leica Geosystem 2016). This instrument is a total station that is able to acquire 1000 points/s with a precision of some millimeters (e.g. 0.002 m at 50 m) when the distance is lower than 200 m. When distance increases beyond 200 m, the measurement frequency is rather lower, even if the level of precision is the same. This instrument is suitable for the survey of reservoirs; usually the reservoir is not fully visible from a single station point, thus it is necessary to create a station network that has to be reciprocally measured. The MultiStation presents high precision in angular measurements (0.3 mgon) that allows reaching high accuracy. Moreover, when surveying loam sediment in a water basin, laser response may be problematic as well (Jaboyedoff et al. 2012; Zamecnikova et al. 2014). In fact, it is affected by the reflective properties of the material (e.g. poorly reflecting or very rough surfaces, parallel incident angles), weather conditions (e.g. rain, hot wind or fog) and environmental light conditions (e.g. a very bright environment). Consequently, materials such as loam or clay decrease the measurement range of EDM (Burton et al. 2011). This method is precise and reliable, with high repeatability if the surveying network is stably materialized in correspondence of the station points. However, this kind of instruments is quite expensive and requires specific surveying knowledge in order to be proficiently used.

A TLS is capable of acquiring precise point clouds in a short period of time. For surveying purposes, laser based on time-of-flight technology is often used. These systems produce from 10,000 to 100,000 points/s, with a precision in the order of 0.01 m at distances of some hundreds of meters (Jaboyedoff et al. 2012). The coordinates of each point are acquired, together with the near-infrared (NIR) radiometric response. These data can be useful to extract information about the type of material or its physical properties (e.g. humidity). In order to correctly georeference the measurements, it is necessary to place within the surveyed scene some targets, characterized by a shape and a material that are useful for manual or automatic marking. Like for total stations, a correct reconstruction of the morphology of a reservoir requires to perform a number of scans from different points of view, in order to overcome the presence of obstacles, which generate omissions in the scan. Then, the different scans can be merged together, creating a single 3D model, thanks to the presence of georeferenced targets and overlapping areas. This task is usually performed using algorithms such as the Iterative Closest Point (ICP) (Chen & Medioni 1991; Besl & McKay 1992). However, the response of the laser light source can be deeply affected by the presence of water and humidity, turning into a reduction of the operative distance of the instrument. This method is less precise and reliable, with respect to the classical topographic methods. On the other hand, it is characterized by repeatability and easiness of use. However, the huge amount of data collected may be difficult to manage.

Digital photogrammetry may represent a low-cost alternative (Jagt et al. 2015). It is based on principles already codified for traditional photogrammetry (Kraus 1993) and it represents a quick and remote 3D acquisition method. Moreover, the images provide a permanent visual recording.

The acquisitions have to be planned carefully because each point has to be visible at least on two frames, for both aerial and terrestrial photogrammetric blocks. The precision of tie points of photogrammetric blocks acquired by UASs cannot be investigated using the traditional rules that can be derived by applying the covariance propagation law to the normal case. Because of the high level of overlapping and the presence of oblique images, the formulas used for close-range photogrammetry could be significant. In fact, in these cases, the number of images and their convergence are fundamental aspects for the computation of the final accuracy. According to Fraser (1992), the precision of an object point $\sigma_{x,\,y,\,z}$ can be expressed as

$$\sigma_{x,y,z} = \frac{q \cdot d \cdot \sigma_i}{f \cdot \sqrt{n}}, \tag{1}$$

where d is the distance between the object and the camera, f is the focal length, n is the number of overlapping images, q is a form factor and σ_i is the precision of the measurements on the images. The latter depends on the measurement principle used, but in case of calibrated cameras, it can be assumed equal to the pixel size. The form coefficient q can be considered equal to 3.5, in case of nadir acquisitions with a standard overlapping equal to 60% of the image size. It decreases to 3 in case of acquisition with high cross-overlapping or to value until 0.4 in case of high convergent geometry. Equation (1) is completely not appropriated in case of UAS photogrammetry with non-metric cameras. However, there is no specific formula to be used in these cases and the close-range case is the most similar, in fact, of camera type and distances from object to camera to the UAS survey. For this reason, the close-range case expression has been applied during the design phase to compute an approximate flight height. This altitude has been reduced by a safety factor equal to 30% taking into account the usage of a model that is not completely suitable for UAS photogrammetry, since it is derived from the close-range case.

For reservoir surveys, the best solution is represented by the use of a camera mounted on aircraft, because the distance between the camera and the object can be maintained in a limited range, avoiding at the same time to have any shadow area. For this kind of surveys, it is very helpful to use UASs (Lucieer et al. 2013; Ouédraogo et al. 2014). If the area to be surveyed is wider than 1 km^2, it is preferable to use fixed wing systems. On the other hand, if the area is smaller, the use of multi-rotor systems has the advantage of vertical takeoffs and landings, which may be very useful in case of steep banks or presence of many obstacles. The overlapping between the images and the strips has to be very high (70%−90% along strip and 60%−90% cross strip) in order to guarantee a multiple intersection of the homologous rays, which in turns allows a precise and reliable survey. The optical sensors installed onboard these systems are mass-market RGB cameras, which must be calibrated in order to remove lens distortions. The parameters recovered with a standard calibration (e.g. using a flat calibration grid) may not be representative of the real camera conditions during the survey, mainly because of the great distance between the sensor and the object (with respect to the one used during the calibration stage) and because of the vibration that the camera can suffer during take-off and landings. For this reason, it is important to refine the internal orientation (IO) parameters performing a self-calibration. The tie points extraction and the measurement of the target positions on the acquired images allow recovering the external orientation parameters of the images that compose the photogrammetric block (Forlani et al. 2015). If the targets are permanently monumented, this last method is precise, reliable and repeatable. Among the methods presented so far, it is the cheapest one, even if it requires trained personnel for both surveying operations and image processing. Furthermore, it requires to measure some GCP in order to correctly georeference the photogrammetric block (Jagt et al. 2015).

3. Fusino dam case study

The case study is the Fusino dam located in Val Grosina (Lombardia region, Northern Italy, see Figure 1). This dam was completed in 1960 and is connected with the Grosio power production

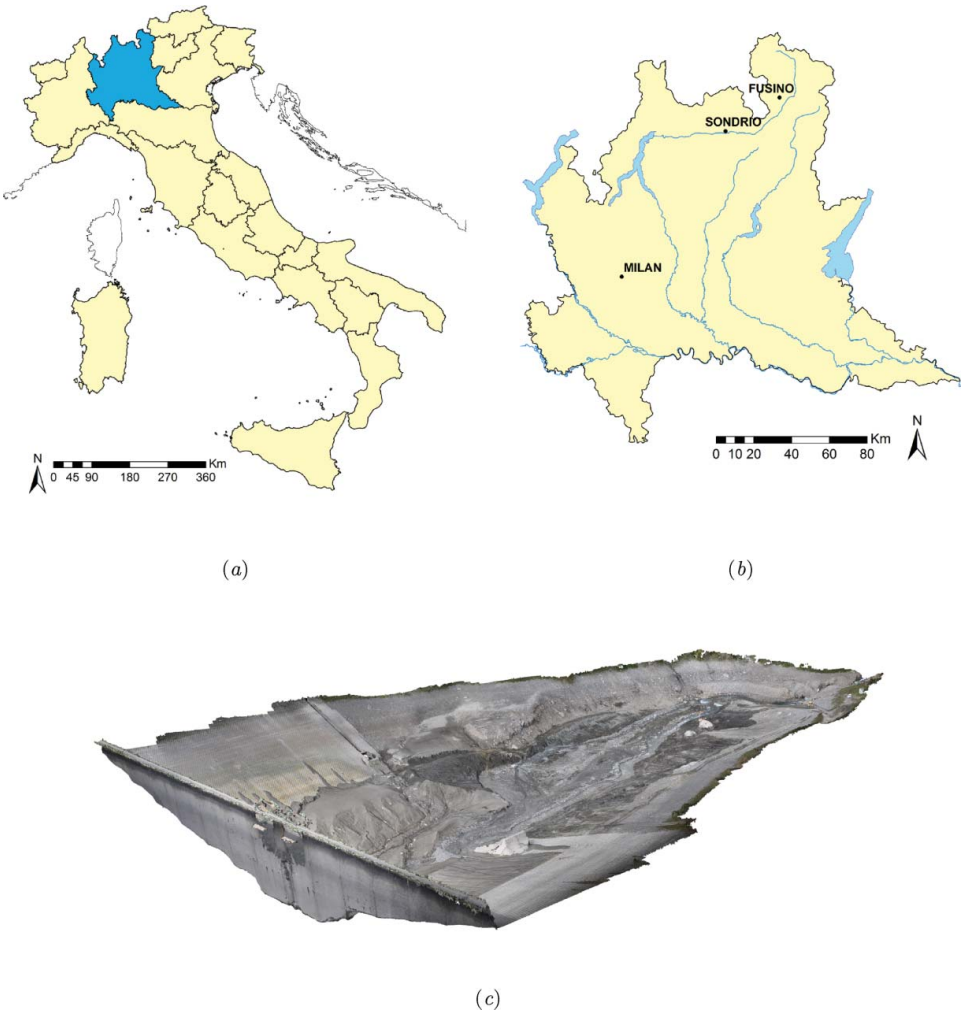

Figure 1. The Fusino dam in Val Grosina, Lombardia region, Northern Italy. (*a*) and (*b*) show the position of the dam, while (*c*) shows the morphology of the surveyed area.

plant. It receives the water from Roasco d'Eita stream and from the penstocks of Roasco di Sanno and Premadio. The dam has a maximum height from ground of 51.50 m, and a total storage of 1.2×10^6 m^3. It is interested by sediment deposition, and the manager authority makes yearly operation of flushing to control the sedimentation and to maintain the storage capacity. In order to evaluate the amount of deposit sediment flushed throughout the dam during the 2015 operations, two different flights have been performed before and after the cleaning operations. The area of the dam was surveyed with a hexacopter UAS by MicroCopter. The system installs onboard a low-cost GPS receiver (Ublox LEA GH), and a triaxial magnetometer and has a maximum payload of 500 g. The case study here presented should be classified in the context of non-critical operations, conducted in Visual Line of Sight (VLoS). For these situations, the regulations of the Italian Civil Aviation Authority (ENAC) require that the pilot is able to maintain a direct eye contact with the UAS. This is necessary to monitor the flight with respect to other aircraft, boats, infrastructure and people in order to avoid collisions. Therefore, the operations in VLoS are allowed up to a maximum horizontal distance of 500 m and a maximum height of 150 m above ground level. Moreover, all the operations must be conducted safely and without harm to third parties. The flights realized at the Fusino dam have been designed following all these regulations.

A very important task for photogrammetry is to carefully plan the survey, considering that it is usually requested to determine the volume of the removed sediments with a tolerance of about 5%−10%, respect to the estimated volume. In the case study, the area interested by flushing is about 45,000 m^2 and during design phase, we estimated a volume of removed sediments of the order of 20,000−30,000 m^3, so the maximum admissible error in the measurement of the height coordinate is about 0.04 m. Consequently, the flight has to be planned in order to obtain an error in the height determination compatible with the requested tolerance. Considering Equation (1), the approximated expected flight height z can be computed. The images have been acquired using a Canon EOS M camera, with a fixed focal length equal to 22 mm. The sensor size is equal to 22.3×14.9 mm^2, with a resolution of 18 Mpixel. We considered σ_{px} equal to 1 pixel (4.384×10^{-6} m), which is a precautionary value considering that the images are processed using automatic algorithm capable of sup-pixel accuracies. Using this data and a form factor q equal to 3, the resulting flight height z is equal to about 140 m, leading to a ground sample distance (GSD) equal to 0.03 m. The value of the form factor has been selected taking into account the high overlapping of the images and the pseudo-nadiral geometry with low intersection angles, which is usually requested from commercial software packages that process images acquired with UASs.

The flight was designed with a maximum height equal to 90 m over the deepest points of the reservoir, which are near the dam. This choice has been performed in order to have a safety factor of 30%, considering that Equation (1) is not completely suitable for UAS surveys. However, the level of the sediment increases going upstream, so the average flight height was equal to 65 m, resulting in an average GSD equal to 0.013 m. Flight plans were organized in 11 strips, with variable length in order to better follow the shape of the basin (see Figure 2). The longest strip was composed of 26 images, while the shortest one (located upstream in correspondence of the tributary inflow) was composed of 11 images. The photogrammetric block has been georeferenced using 22 GCPs. In Figure 3(*a*), it is possible to see that the distribution of point is not the optimal one. In fact, at the centre of the reservoir, no GCP is available. Unfortunately, this area cannot be reached to put targets because of the presence of mud. Each point has been marked with a square target of

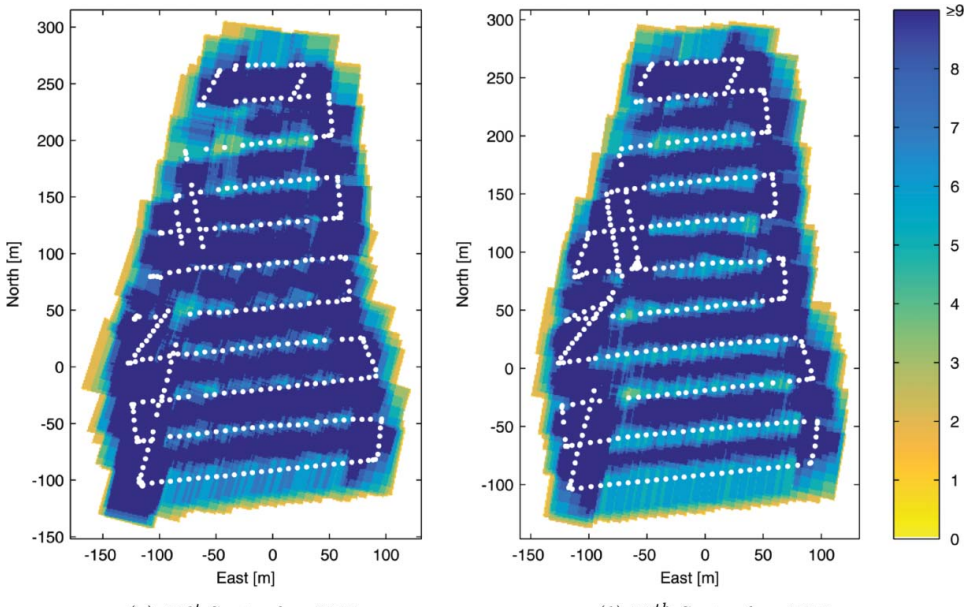

(*a*) 21^{st} September 2015 (*b*) 30^{th} September 2015

Figure 2. Camera locations (white dots) and image overlapping (colour bar) for each of the two surveys. **To view this figure in colour, see the online version of the journal.**

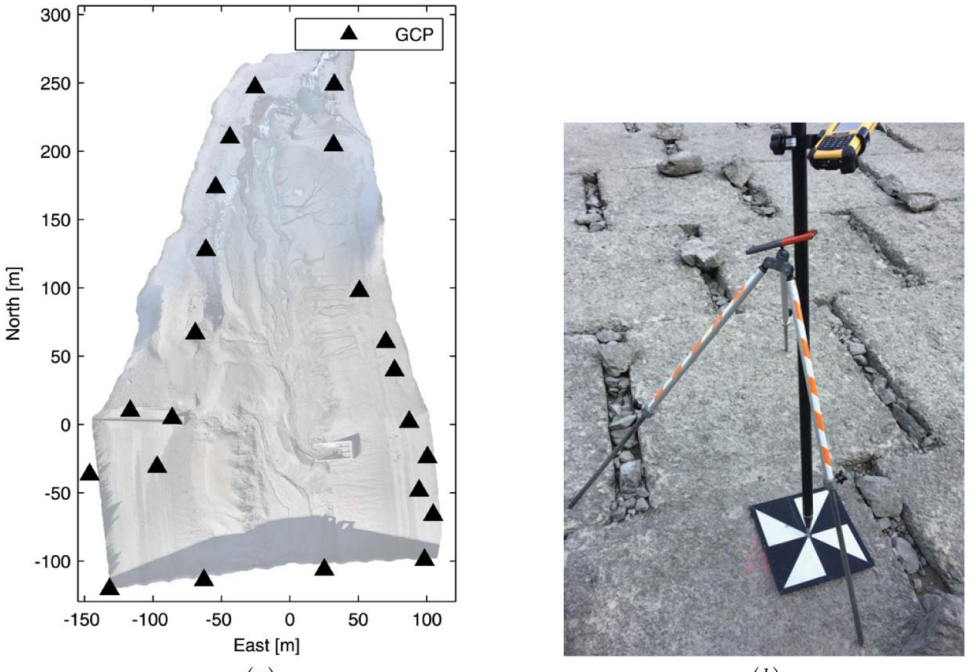

Figure 3. (*a*) GCPs distribution in the surveyed area. (*b*) Example of target used for GCPs monumentation and their measurement with RTK-GNSS.

size 0.30 × 0.30 m^2 made of alternative black and white triangles, as shown in Figure 3(*b*). Each GCP has been materialized and measured both with RTK-GNSS and classical topographic methods. In the first case, each point was surveyed with a dual-frequency GNSS receiver with the antenna mounted on a pole. The receiver is able to work in RTK mode, using the differential correction send by NETGEO permanent network (Topcon Positioning Italy S.r.l. 2015). Each point is the average of three measurement epochs acquired on it, leading to an accuracy of some centimetres (standard deviation of 0.02 m in the horizontal directions and 0.05 cm in the vertical coordinate). In the second case, a geodetic network composed of three stations located on three GCPs was built. From each station, all the visible GCPs were measured, thus guarantying high redundancy and precision in the final adjustment. The accuracy of estimated coordinates was about 0.01 m in all the directions. Moreover, some stations of the geodetic network used in the validation phase (that will be explained in the following) was observed, thus ensuring to have the same global reference frame. The images were processed using the Agisoft Photoscan software (version 1.2.2). The first block was acquired on 21st September before flushing operations, and it is composed by 324 images. The second block was acquired on 30th September and is composed by 369 frames. The images of each flight have been processed separately, following the standard workflow proposed by the software. The marker accuracy has been imposed equal to 1 pixel, considering this value representative of the operator's accuracy, while the tie points accuracy has been left equal to the default value of 4 pixels. The accuracy of each GCP was specified, in accordance to the precision reached during the surveying phase. Due to the fact that the software allows inserting a single value for the accuracy of a point (instead of specifying it for each coordinate), a 3D accuracy was computed. For RTK-GNSS network, the values of the precisions directly computed by the receiver have been used, while for the geodetic network, we have used the precisions computed during the adjustment of the network. These

Table 1 RMSE between the GCP measured coordinates and the estimated ones.

	GNSS GCP			Total station GCP		
Flight date	East (m)	North (m)	Up (m)	East (m)	North (m)	Up (m)
21st September	0.022	0.019	0.022	0.003	0.003	0.004
30th September	0.023	0.019	0.021	0.005	0.004	0.007

accuracies have been used in the bundle block adjustment to correctly weigh the different observations. Each photogrammetric block has been oriented considering the coordinates of GCPs measured both with GNSS-RTK and total station. The corresponding empirical accuracies are reported in Table 1. They represent the root mean square error (RMSE) between the measured and the estimated coordinates. After recovering the external orientation parameters, we used the 'optimize stage' of PhotoScan to perform the camera self-calibration. This step is fundamental in case of image blocks acquired from UAS, because the lens are suffering impacts during the take-off and landing operations, that could modify the IO parameters estimated during a standard calibration step. Then, the two dense point clouds have been reconstructed using a medium point density, which corresponds to downscaling the input image size by a factor of 16. The output dense point clouds are approximatively composed of 40 million points.

The DSM reckoned with the use of photogrammetry was validated by comparing it with some sample points measured with the robotic total station Leica TS-30. This technique guarantees high accuracy and relatively automatized observations. In fact, the instrument has an onboard software that allows automatic scan of a surface on a regular angular grid. Leica TS-30 has high accuracy in angle measurement (0.3 mgon of std.) as well as a very precise EDM that is able to measure without the use of a reflector. Thus, it was possible to measure points on the bottom of the reservoir without having direct access. Due to the presence of sunlight reflection on water in the mud, it was not possible to measure distances greater than 150−200 m, although the EDM is designed for 1000 m distances. This limitation leads to observe the reservoir from different points of view and so it was required to build a network and then adjust all the observations together. In particular, a network of five stations was built, but only four of them were used to measure grids of points (see Figure 4). The same stations were used for both the surveys, allowing consistency between the two epochs. Moreover, two stations were observed with GPS static measurements in order to ensure the same North direction in adjustment of the two surveys. The final coordinates of points have been computed with the open-source GeoNet software (Rossi et al. 2012; GeoNet 2015), developed at Politecnico di Milano. It is able to perform rigorous least square adjustment of integrated geodetic network (GPS and Total Station) directly in the global reference frame, considering vertical deflection from the geoid model ITALGEO2005 (Albertella et al. 2008). The estimated coordinates of station points of the network and the residuals between the two epochs are shown in Tables 2−4. In order to verify that the reference system was stably materialized, a statistical test on the position of network stations has been performed. The hypothesis is that each coordinate of each station is the same for the two different epochs. According to Albertella et al. (2006), the statistic of the test is

$$t_{exp} = \frac{|X_1 - X_2|}{\sqrt{\sigma_{X1}^2 - \sigma_{X2}^2}} \sim t_{n-m,\alpha}, \tag{2}$$

where X_1 and X_2 represent a generic coordinate at the two different epochs, ${\sigma^2}_{X1}$ and ${\sigma^2}_{X2}$ their variance, and $n - m$ the redundancy of least squares adjustment, performed using the GeoNet software. Due to the fact that the design of the two networks is slightly different (but we consider it the same), as a safety factor, the maximum between the two redundancy is used, thus the $t_{n\,-\,m,\,\alpha}$ value is 1.99, assuming the significance level $\alpha = 5\%$. Columns 5, 6, and 7 of Table 4 report the computed empirical value of t_{exp} that results always smaller than the threshold value. This means that the hypothesis of consistency between the reference frame of the two epochs is verified.

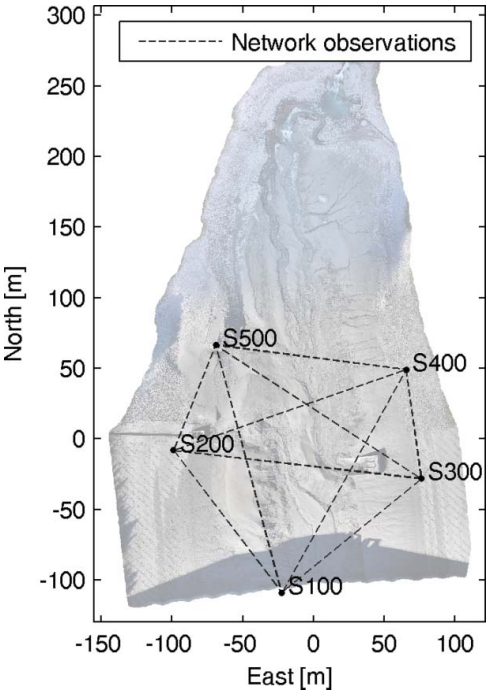

Figure 4. Design of network used to determine the coordinates of station points. Notice that validation points are measured from station S200, S300, S400, and S500, while S100 is used only in order to add redundancy to the adjustment of this network.

Table 2 Estimated coordinates of the station points on 21st September.

Point	East (m)	North (m)	Up (m)	Sd. East (mm)	Sd. North (mm)	Sd. Up (mm)
S100	−22.412	−108.964	10.397	5.7	4.3	10.0
S200	−99.093	−8.190	−8.609	9.6	4.7	11.0
S300	76.244	−28.298	−7.172	4.3	3.5	10.2
S400	65.264	49.123	−4.887	4.6	7.4	10.6
S500	−69.075	66.534	−7.785	8.1	8.4	10.8

Table 3 Estimated coordinates of the station points on 30th September.

Point	East (m)	North (m)	Up (m)	Sd. East (mm)	Sd. North (mm)	Sd. Up (mm)
S100	−22.412	−108.964	10.399	4.6	3.6	8.1
S200	−99.093	−8.191	−8.603	7.6	3.5	8.1
S300	76.244	−28.298	−7.174	3.5	2.9	8.1
S400	65.265	49.123	−4.883	3.5	5.5	8.1
S500	−69.083	66.531	−7.782	6.4	6.2	8.2

Table 4 Differences between the coordinates of the station points estimated at the two epochs.

Point	ΔEast (mm)	ΔNorth (mm)	ΔUp (mm)	t_{exp} East	t_{exp} North	t_{exp} Up
S100	−0.2	0.0	1.5	0.027	0.002	0.116
S200	0.2	−0.4	5.8	0.014	0.062	0.428
S300	0.2	0.2	−2.1	0.035	0.033	0.158
S400	0.2	−0.2	4.5	0.039	0.019	0.336
S500	−8.0	−2.9	2.5	0.773	0.274	0.187

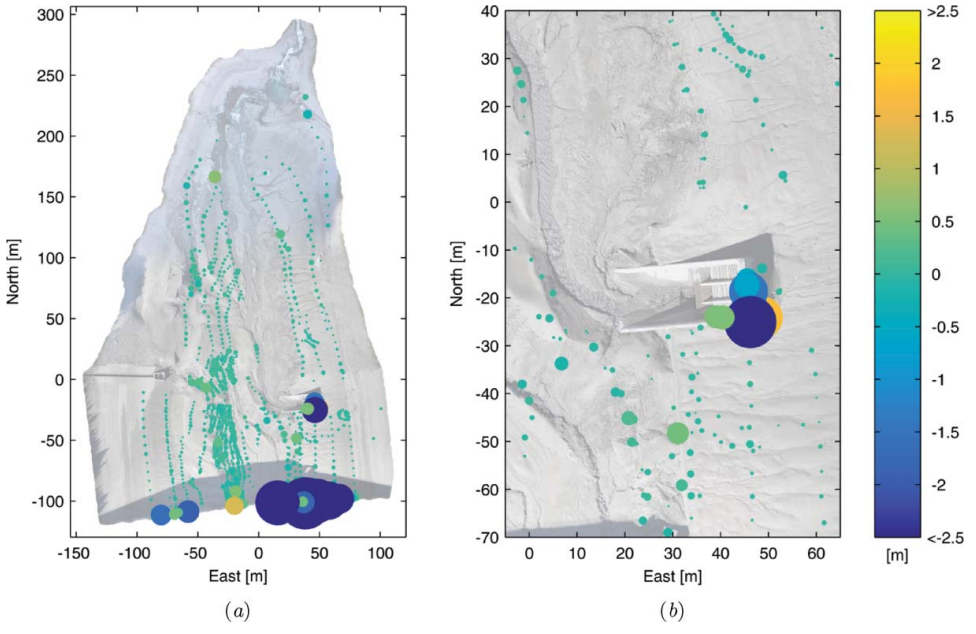

Figure 5. Differences between the DSM estimated with the photogrammetric survey and the validation dataset on 21st September 2015. The circle size increases with the difference between the two measurements. (*a*) refers to the entire reservoir, while (*b*) focuses on an example of an area with suddenly DSM variations.

Note that all the results have been roto-translated in a local Cartesian coordinate system whose origin is in the point with ETRF2000 coordinates equal to $X = 4342471.390$ m, $Y = 785056.528$ m, $Z = 4591427.410$ m. This has been done because it allows obtaining better results during the photogrammetric processing, even if all the networks were adjusted directly in the global reference frame, as already explained. In order to validate the DSM estimated with the photogrammetric survey, it has been compared with the point cloud measured with the total station. The differences between the total station point cloud and the photogrammetric-based DSM, computed for the 21st September survey, are shown in Figure 5(*a*), where it is possible to see that there are some high inconsistencies located where there are abrupt variations in the DSM. If the absolute value of the difference in a point was greater than 0.40 m, we assumed that the point measured with the total station was not the same represented in the DSM as shown in Figure 5(*b*) (e.g. in case of a wall, DSM could represent the base and total station could observe the top, or vice versa). These points were considered outliers and removed from the validation dataset. In total, we measured 1148 points during the survey of 21st September and 440 points for the survey of 30th September. However, according to this criterion, less than 1% of points were classified as outliers in both cases. Figure 6 shows the histograms of the results of the validation for the two different epochs, once outliers were removed. Both the cases had an almost zero mean and a standard deviation of about 0.05 m as shown in Table 5. The volume of sediments that has been flushed away from the reservoir can be easily computed according to Equation (3):

$$\Delta V = \sum_{i=1}^{N} A_i \left(z_i^{t1} - z_i^{t2} \right), \tag{3}$$

where N is the number of DSM cell (about 262 milions), ${z^{t1}}_i$ and ${z^{t2}}_i$ are the height associated to each cell of the DSM at the two different epochs, respectively. Overall, about 2.6×10^5 m^3 were removed during the week between 21st and 30th September.

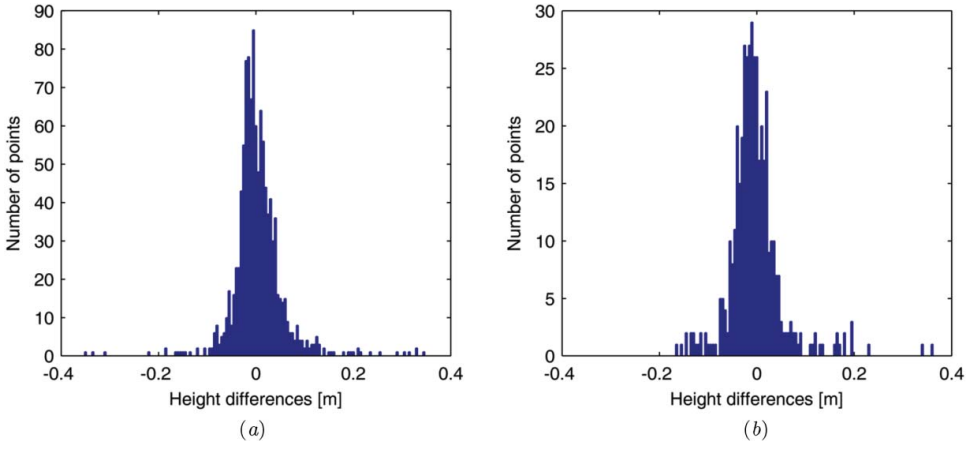

Figure 6. Histograms of the residuals between DSMs and validation dataset. (*a*) 21st September 2015 (1109/1148 points used for the histogram), (*b*) 30th September 2015 (435/440 points used for the histogram).

In Figure 7, the differences between the DSMs of the two epochs are represented. This figure highlights the area where sediments were removed. In order to compute the accuracy of volume determination, the field of residual between the total station point cloud and the DSM was used also to model empirically the covariance of the error of DSM (Papoulis 1977; De Gaetani et al. 2015), assuming that the error is spatially isotropic and homogeneous at each epoch. Thus, two covariance matrices C_1 and C_2 can be computed for the DSM at each time and the variance of the volume difference can be computed as

$$\sigma^2_{\Delta V} = \begin{bmatrix} \mathbf{e}^t & -\mathbf{e}^t \end{bmatrix} \begin{bmatrix} C_1 & 0 \\ 0 & C_2 \end{bmatrix} \begin{bmatrix} \mathbf{e} \\ -\mathbf{e} \end{bmatrix} = \mathbf{e}^t C_1 \mathbf{e} + \mathbf{e}^t C_2 \mathbf{e}, \tag{4}$$

where $\mathbf{e}$ is a vector with all components equal to 1 and length equal to the number of pixel N of the DSM at one epoch. The characteristic of C_1 and C_2 is to be spatially invariant and, according to the data, $C_1 = C_2 = C$, thus each product $\mathbf{e}^t C \mathbf{e}$ can be seen as a convolution integral. Using the 2D Fourier transform, it is easy to reckon the result applying the convolution theorem (Papoulis 1977), that allows to compute this huge matrix product in less than 10 s, on a common personal computer. The final estimated standard deviation of the volume difference is about 280 m^3, that is, about the 1% of the removed volume.

The UAS-based survey allows to reconstruct the elevation−volume curve for the reservoir. We have determined this curve before and after the sediments removal (reported in Figure 8), together with a previous estimation of the same curve realized in 1974 by the company managing the dam. From Figure 8, it is possible to see that sedimentation has a strong impact on the total volume of water stored in the reservoir. In fact, the volume of water that can be stored nowadays is less than the one that could be stored in 1974, at a given height. As expected, sediments effect is stronger for low water elevations. This is clearly due to the fact that sediments occupy the base of the reservoir. We quantify the effect of sediments on the reservoir capacity by calculating the absolute difference

Table 5 Mean and standard deviation of the residuals between each DSM and validation dataset.

Date	Mean	Std. Dev.
21st September	0.003 m	0.054 m
30th September	−0.004 m	0.053 m

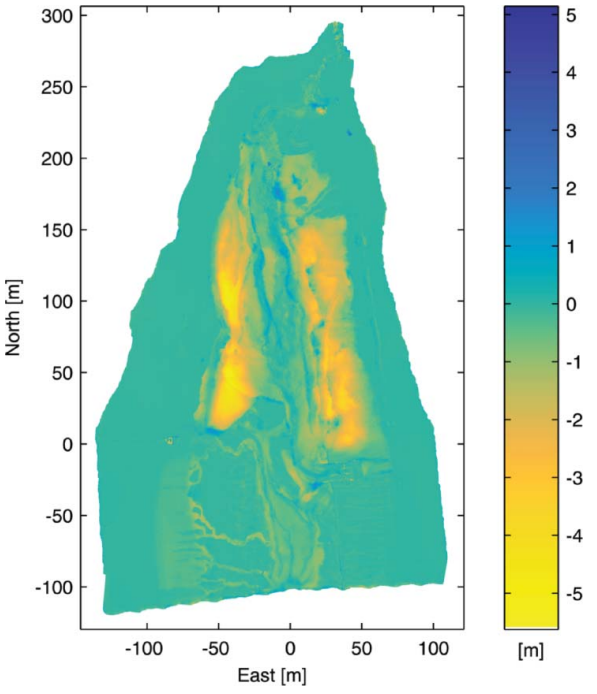

Figure 7. Excavated volume computed as difference between the two estimated DSMs.

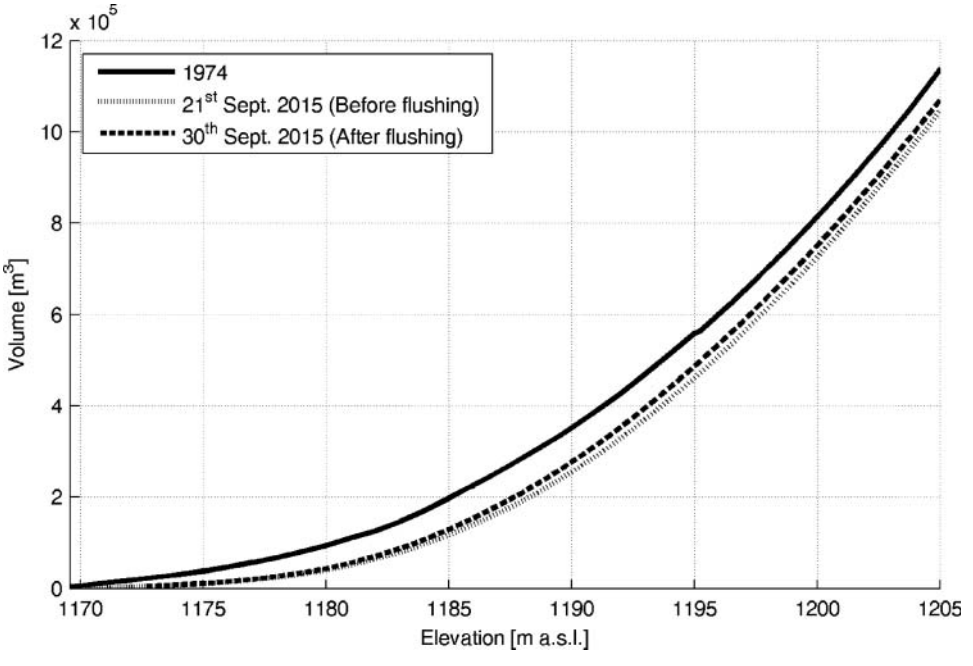

Figure 8. Elevation–volume curves for the reservoir, derived from the estimated DSMs (before and after sediment excavation), compared to the elevation–volume curve corresponding to 1974.

between the maximum volume that can be stored nowadays (after the sediment removal, V_{2015}) and the volume that could be stored in 1974 (V_{1974}), as a relative quantity with respect to V_{1974} (ΔV):

$$\Delta V = \left| \frac{V_{2015} - V_{1974}}{V_{1974}} \right| \tag{5}$$

is equal to 6% (calculated in correspondence of 1205 m a.s.l.).

4. Conclusions and final remarks

Here, we have estimated the volume of flushed sediments in an alpine reservoir (the Fusino dam, located in Lombardia region, Northern Italy) using two UAS-based photogrammetric surveys. This volume was evaluated comparing two DSMs, before and after flushing operations, calculated from images acquired with UAS surveys. The two flights were realized at an average flight height of 65 m. This leads to a mean GSD of 0.013 m. The RMSE between the measured and the estimated GCP coordinates are coherent with the results obtained by other authors using multi-temporal images collected from UAS for DSM estimation (e.g. Rosnell et al. (2011)). In case of GCP measured with the total station, the results are comparable with those obtained by Nocerino et al. (2013), even if in that case they used a professional full-frame reflex camera, and thus GSD was smaller. The performances of digital photogrammetry were validated using the data collected with a robotic total station. The validation dataset has almost zero mean and a standard deviation of about 0.05 m, which cannot be considered a purely white noise, and thus the correlation is modelled empirically. Our validation results are similar to those obtained by Dall'Asta et al. (2015). In their case, the elevation discrepancies between GCPs measurements and photogrammetric surface reconstruction were in the order of 0.10−0.15 m, but the GSD was wider. This validation supports the volume of sediments obtained using two UAS surveys.

Digital photogrammetry with UAS allowed reconstructing the surface of the reservoir with a high level of detail: 40 million of points, which correspond to about 500 points/m^2. Each flight required about 6 hours for the survey and almost 1.5 days for data post-processing. Clearly, the duration of post-processing is dependent on the number of images composing the photogrammetric block, as well as on the performances of the computer used. Anyway, these requests prove that digital photogrammetry from UAS is a fast and cheap way to retrieve the data needed by these applications. Nevertheless, the method presents some problematic issues. In fact, from the regulatory point of view, the authorization required to fly are more and more restrictive. In Europe, there are strong constraints on the maximum relative flight height (that usually does not exceed 150 m) and on the maximum action range, namely the maximum distance of the UAS from the takeoff point (usually maximum 500 m, depending on the kind of UAS). Furthermore, piloting the UAS requires a particular flying license, issued by national civil aviation authorities (e.g. in Italy, ENAC). The orography of the surveyed area could represent a further limitation. In fact, if the basin lies in a mountain area where steep slopes are present, only multirotor UAS can be used, because of their capability to takeoff and landing vertically, thus minimizing the space required for these operations. On the other hand, this kind of UAS has a scarce flight autonomy with respect to fixed-wing UAS that, instead, requires a wider area to land, takeoff and to change direction, not always available in alpine scenarios. It is worth to notice that, in order to perform the flight planning and the photogrammetric data processing, an expert operator is required, and that in any case, a traditional or GNSS topographic survey of the GCP is required.

Each photogrammetric block has been processed twice, using as coordinates of the GCPs those estimated using RTK-GNSS, and those computed from the classical topographic measurements. The differences in the photogrammetric bundle block adjustment are negligible showing that even a RTK-GNSS survey may be sufficient to reach the requested tolerance. Clearly, satellite visibility is an

important requirement that must be considered when planning the GNSS measurements. Main advantages of a RTK-GNSS survey with respect to classical topographic methods are during surveying phase: it is faster, cheaper and easier to use than classical topographic survey.

From a hydrological point of view, sedimentation represents a key issue for alpine reservoirs, since it reduces the regulation capacity and the volume of the reservoir. Thus, the flushing of sediments is a practice used to restore the capacity of reservoir. The volume of flushed sediments was estimated to be about 26,000 m^3, which represents about 2%−3% of the total capacity. The impact of sediments on the reservoir capacity was assessed calculating the absolute difference between the maximum volume that can be stored nowadays within the reservoir (after the sediments removal), and the volume that could be stored about 40 years ago (i.e. reservoir practically without sediments). For this case study, we found that this difference is equal to 6% (at 1205 m a.s.l.). The reduction of available volume in a reservoir is a living topic that constitutes an economical and environmental risk. This is particularly true in conditions of soil degradation due to climate change.

Acknowledgements

We would to thank Concetto Spennati of Teorema Topcenter s.r.l. for the technical and instrumental support and the students of the Summer School of Politecnico di Milano 'Design and realization of topographic surveying' Alberto Agnoletti, Romina Anesi, Mattia Anghileri, Gabriele Antinucci, Marco Bosisio, Alessandro Mattiroli, and Giulia Scelsi who keenly participated in the surveying operations.

Disclosure statement

No potential conflict of interest was reported by the authors.

References

Alba M, Fregonese L, Prandi F, Scaioni M, Valgoi P. 2006. Structural monitoring of a large dam by terrestrial laser scanning. Int Arch Photogramm Remote Sens Spat Inf Sci. 36:6.

Albertella A, Barzaghi R, Carrion D, Maggi A. 2008. The joint use of gravity data and GPS/levelling undulations in geoid estimation procedures. Bollettino di Geodesia e Scienze Affini Istituto Geografico Militare, Florence. 67:49−59.

Albertella A, Cazzaniga N, Sansò F, Sacerdote F, Crespi M, Luzietti L. 2006. Deformations detection by a Bayesian approach: prior information representation and testing criteria definition. In: Geodetic deformation monitoring: from geophysical to engineering roles, volume 131 of International Association of Geodesy Symposia. Springer; p. 30−37.

Annandale GW. 1987. Reservoir sedimentation. Amsterdam: Elsevier.

Basson G. 2010. Sedimentation and sustainable use of reservoirs and river systems. International Commission on Large Dams (ICOLD) Bulletin. Available from: http://www.icold-cigb.org/userfiles/files/CIRCULAR/CL1793Annex.pdf

Besl PJ, McKay ND. 1992. Method for registration of 3-d shapes. Proceedings of the SPIE 1611, Sensor Fusion IV: Control Paradigms and Data Structures, 586; 1992 Apr 30. Available from: http://dx.doi.org/10.1117/12.57955

Brune GM. 1953. Trap efficiency of reservoirs. Eos Trans Am Geophys Union. 34:407−418.

Burton D, Dunlap DB, Wood LJ, Flaig PP. 2011. Lidar intensity as a remote sensor of rock properties. J Sediment Res. 81:339−347.

Chen Y, Medioni G. 1991. Object modeling by registration of multiple range images. In: 1991 IEEE International Conference on Robotics and Automation; 1991. Proceedings. IEEE; p. 2724−2729. Sacramento, CA.

Churchill M. 1948. Discussion of "Analysis and use of reservoir sedimentation data". In: Proceedings of the Federal Interagency Sedimentation Conference. Washington (DC): Bureau of Reclamation, US Department of the Interior; p. 139−140.

Clarke TA. 1994. Analysis of the properties of targets used in digital close-range photogrammetric measurement. Proceedings of SPIE - The International Society for Optical Engineering 2350; p. 251−262.

Dall'Asta E, Delaloye R, Diotri F, Forlani G, Fornari M, di Cella UM, Pogliotti P, Roncella R, Santise M. 2015. Use of uas in a high mountain landscape: the case of gran sommetta rock glacier (ao). ISPRS-Int Arch Photogrammetry, Remote Sensing Spat Inf Sci. 1:391−397.

De Gaetani CI, Cazzaniga NE, Barzaghi R, Reguzzoni M, Betti B. 2015. Covariance function modelling in local geodetic applications using the simplex method. Boll Ciências Geodésicas (in print).

Dunbar JA, Allen PM, Higley PD. 1999. Multifrequency acoustic profiling for water reservoir sedimentation studies. J Sediment Res. 69:518–527.
Fonstad MA, Dietrich JT, Courville BC, Jensen JL, Carbonneau PE. 2013. Topographic structure from motion: a new development in photogrammetric measurement. Earth Surf Process Landforms. 38:421–430.
Forlani G, Roncella R, Nardinocchi C. 2015. Where is photogrammetry heading to? State of the art and trends. Rend Lincei. 26: 1–12.
Fraser CS. 1992. Photogrammetric measurement to one part in a million. Photogramm Eng Remote Sens. 58:305–310.
Fruchard F, Camenen B. 2012. Reservoir sedimentation: different type of flushing-friendly flushing example of genissiat dam flushing. In: ICOLD International Symposium on Dams for a Changing World; Kyoto, Japan; p. 1–6.
Furnans J, Austin B. 2008. Hydrographic survey methods for determining reservoir volume. Environ Model Softw. 23:139–146.
GeoNet. 2015. [Internet]; [cited 2015 Nov 3]. Available from: http://sourceforge.net/projects/geonet/
González-Aguilera D, Gómez-Lahoz J, Sánchez J. 2008. A new approach for structural monitoring of large dams with a three-dimensional laser scanner. Sensors. 8:5866–5883.
Graf WL. 1999. Dam nation: a geographic census of american dams and their large-scale hydrologic impacts. Water Resour Res. 35:1305–1311.
Hallet B, Hunter L, Bogen J. 1996. Rates of erosion and sediment evacuation by glaciers: a review of field data and their implications. Global Planet Change. 12:213–235.
Jaboyedoff M, Oppikofer T, Abellán A, Derron MH, Loye A, Metzger R, Pedrazzini A. 2012. Use of lidar in landslide investigations: a review. Nat Hazards. 61:5–28.
Jagt BV, Lucieer A, Wallace L, Turner D, Durand M. 2015. Snow depth retrieval with UAS using photogrammetric techniques. Geosciences. 5:264–285.
Jansson MB, Erlingsson U. 2000. Measurement and quantification of a sedimentation budget for a reservoir with regular flushing. Regul Rivers Res Manag. 16:279–306.
Kondolf GM, Gao Y, Annandale GW, Morris GL, Jiang E, Zhang J, Cao Y, Carling P, Fu K, Guo Q, et al.. 2014. Sustainable sediment management in reservoirs and regulated rivers: experiences from five continents. Earth Future. 2:256–280.
Kraus K. 1993. Photogrammetry: vol. 1, fundamentals and standard processes. Cologne: Ferdinand Dummlers Verlag.
Kummu M, Varis O. 2007. Sediment-related impacts due to upstream reservoir trapping, the lower mekong river. Geomorphology. 85:275–293.
Leeder MR, Harris T, Kirkby MJ. 1998. Sediment supply and climate change: implications for basin stratigraphy. Basin Res. 10:7–18.
Leica Geosystem. 2016. [Internet]; [cited 2016 Apr 19]. Available from: http://leica-geosystems.com/products/total-stations/multistation/leica-nova-ms60
Lewis SE, Bainbridge ZT, Kuhnert PM, Sherman BS, Henderson B, Dougall C, Cooper M, Brodie JE. 2013. Calculating sediment trapping efficiencies for reservoirs in tropical settings: a case study from the Burdekin falls dam, NE Australia. Water Resour Res. 49:1017–1029.
Lucieer A, de Jong S, Turner D. 2013. Mapping landslide displacements using structure from motion (SFM) and image correlation of multi-temporal UAV photography. Prog Phys Geogr. 38:97–116.
Mahmood K. 1987. Reservoir sedimentation: impact, extent, and mitigation. Washington, DC: International Bank for Reconstruction and Development. (Technical paper. Report no. WTP71)
Morris GL, Fan J. 1998. Reservoir sedimentation handbook: design and management of dams, reservoirs, and watersheds for sustainable use. New York: McGraw Hill Professional.
Nocerino E, Menna F, Remondino F, Saleri R. 2013. Accuracy and block deformation analysis in automatic UAV and terrestrial photogrammetry – lesson learnt. Int Arch Photogram Remote Sens Spat Inf Sci. 5:W1.
Ouédraogo MM, Degré A, Debouche C, Lisein J. 2014. The evaluation of unmanned aerial system-based photogrammetry and terrestrial laser scanning to generate DEMs of agricultural watersheds. Geomorphology. 214:339–355.
Owens P, Batalla R, Collins A, Gomez B, Hicks D, Horowitz A, Kondolf G, Marden M, Page M, Peacock D, et al.. 2005. Fine-grained sediment in river systems: environmental significance and management issues. River Res Appl. 21:693–717.
Palmieri A, Shah F, Annandale G, Dinar A. 2003. Reservoir conservation volume I: the RESCON approach, economic and engineering evaluation of alternative strategies for managing sedimentation in storage reservoirs. A contribution to promote conservation of water storage assets worldwide. Washington (DC): The International Bank for Reconstruction and Development.
Papoulis A. 1977. Signal analysis. Vol. 191. Michigan: McGraw-Hill.
Poff NL, Hart DD. 2002. How dams vary and why it matters for the emerging science of dam removal an ecological classification of dams is needed to characterize how the tremendous variation in the size, operational mode, age, and number of dams in a river basin influences the potential for restoring regulated rivers via dam removal. BioScience. 52:659–668.

Roncella R, Re C, Forlani G. 2011. Comparison of two structure and motion strategies. ISPRS-Int Arch Photogramm Remote Sens Spat Inf Sci. 3816:343–350.
Rosnell T, Honkavaara E, Nurminen K. 2011. On geometric processing of multi-temporal image data collected by light UAV systems. Int Arch Photogramm Remote Sens Spat Inf Sci. 38:1–6.
Rossi L, Sampietro D, Sansò F. 2012. Geonet: un software per la compensazione di reti topografiche integrate [Geonet: a software for integrated geodetic network adjustment]. In: atti 16a conferenza nazionale Asita; 6–9 novembre 2012; Vicenza; p. 1157–1164.
Skarlatos DP, Vlachos M, Vamvakousis V. 2015. Investigating influence of UAV flight patterns in multi-stereo view DSM accuracy. In: Remondino F, Shortis MR, editors. Proceedings of SPIE Vol. 9528: Videometrics, Range Imaging, and Applications XIII; p. 95280M–95280M.
Surian N, Ziliani L, Comiti F, Lenzi MA, Mao L. 2009. Channel adjustments and alteration of sediment fluxes in gravel-bed rivers of north-eastern Italy: potentials and limitations for channel recovery. River Res Appl. 25:551–567.
Topcon Positioning Italy Srl. 2015. [Internet]; [cited 2015 Nov 3]. Available from: http://www.netgeo.it/; website
Trimble SW, Bube KP. 1990. Improved reservoir trap efficiency prediction. Environ Profess. 12:255–272.
Van Metre PC, Callender E, Fuller CC. 1997. Historical trends in organochlorine compounds in river basins identified using sediment cores from reservoirs. Environ Sci Technol. 31:2339–2344.
Westoby M, Brasington J, Glasser N, Hambrey M, Reynolds J. 2012. 'Structure-from-motion' photogrammetry: a low-cost, effective tool for geoscience applications. Geomorphology. 179:300–314.
Yang S, Milliman J, Li P, Xu K. 2011. 50,000 dams later: erosion of the Yangtze river and its delta. Global Planet Change. 75:14–20.
Zamecnikova M, Neuner HB, Pegritz S. 2014. Influence of the incidence angle on the reflectorless distance. In: INGEO 2014 – Proceedings of the 6th International Conference on Engineering Surveying; 2014 Mar 3–Mar 4. Prague: Czech Technical University Prague, Faculty of Civil Engineering; p. 257–262.
Zhou Z. 1993. Remarks on reservoir sedimentation in China. In: Fan SS, Morris G, editors. Notes on Sediment Management in Reservoirs: National and International Perspectives. Washington, DC: Federal Energy Regulatory Commission.